Chapter 2 *Synthesis and Characterization techniques*

2.1 Introduction

Perovskite oxides can be synthesized by several synthesis techniques such as solid-state reaction, co-precipitation, sol-gel, hydrothermal, high-energy ball milling, *etc*. These different synthesis methods although produce the perovskite oxides with the same phase and stoichiometry, their properties, however, may vary significantly depending upon the microstructure (shape and size) of synthesized particles. So, the selection of synthesis method is an important step to have desired microstructure and properties. In the present work, a facile and cost-effective solution combustion method is adopted to synthesize the pristine $CeCrO_3$ and Fe doped $CeCrO_3$ nanoparticles which is discussed in section 2.2. The working principle and operational details of different characterization techniques are discussed in section 2.3.

2.2 Sample preparation

Traditionally, most perovskite ceramic materials have been synthesized using a solid-state reaction, which involves mixing their constituent oxides and heating them to a high temperature (often between 1000 and 1500°C). However, this method results in samples with low homogeneity and large particle size due to impurities and secondary phases introduced during the manual grinding and ball milling process [98]. Alternative synthetic methods include wet chemical routes, such as sol-gel, hydrothermal, and co-precipitation methods, as well as

combustion synthesis. Combustion synthesis, also known as the self-propagating method, is a highly efficient and simple method for producing perovskite oxide powders and various other industrial materials. This process involves a highly exothermic self-combustion reaction between a fuel (usually glycine or urea) and oxidizers (e.g., metal nitrates) [99,100]. Compared to the solid-state reaction method, combustion synthesis offers several benefits, such as better homogeneity and smaller particle size.

2.2.1 Solution combustion

$CeCr_{1-x}Fe_xO_3$ ($0 \leq x \leq 0.5$) samples were prepared via glycine nitrate solution combustion method, employing analytical grade of $Ce(NO_3)_3 \cdot 4H_2O$ (Himedia, >99.9%), $Cr(NO_3)_3$(Himedia,>99.9%), $Fe(NO_3)_3$(Himedia, >99.9%) and glycine (NH_2CH_2COOH) as the precursor materials. To synthesize of $CeCrO_3$, $Ce(NO_3)_3$ and $Cr(NO_3)_3$ were taken in stoichiometric ratio and dissolved in 30 ml double distilled water, along with glycine (NH_2CH_2COOH). The metal to glycine ratio was maintained at 1:1:3.33. The solution was heated with magnetic stirring on a hot plate at 80 °C for 30 minutes. Subsequently, the temperature was increased to 350 °C to initiate combustion. Auto-combustion occurred during the heating process, resulting in the formation of a voluminous powder. The powder was then held at 300 °C for a duration of two hours. To create the Fe-doped sample, *x* at% of $Cr(NO_3)_3$ (Himedia, purity >99.9%) was substituted with an equal quantity of $Fe(NO_3)_3$ (Sigma Aldrich, purity >99.9%), using a similar synthesis procedure. The resulting fluffy powder was ground for one hour and subsequently utilized for characterization purposes.

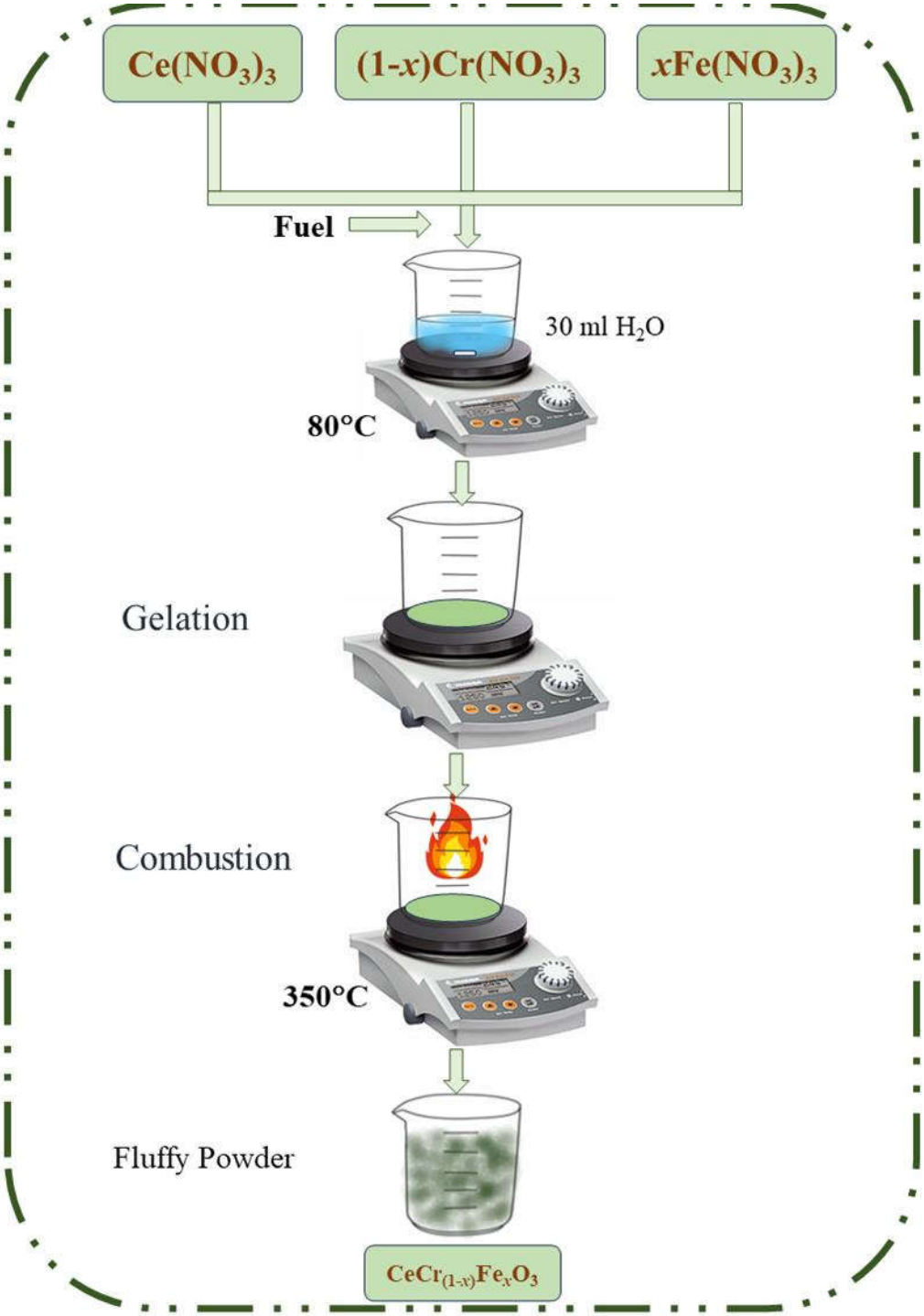

Figure 2.1 Pictorial representation for the synthesis of $CeCr_{1-x}Fe_xO_3(0\leq x\leq 0.5)$ using combustion method.

2.3 Characterizations

In order to systematically study the structure, optical and magnetic properties of pristine and Fe doped $CeCrO_3$ powder samples, different characterization techniques have been used in the present work. A brief discussion on these characterization techniques is given below.

2.3.1 X-ray diffraction (XRD)

X-ray diffraction (XRD) is a non-destructive characterization technique which is widely adopted to determine the phase, purity, and the crystal structure of a particular material. This technique works on the famous Bragg's law of diffraction proposed by W. H. Bragg and his son W. L. Bragg. According to Bragg's law, when a monochromatic beam of x-rays incident on a set of equally spaced crystal planes, the constructive interference of the diffracted x-rays could occur only after the fulfillment of the following two conditions. First, the angle of incidence of x-rays must be equal to the diffraction angle. Second, the path difference between the incident and diffracted x-rays must be an integral multiple of the x-ray wavelength. Bragg's law is expressed as

$$2d\sin\theta = n\lambda \qquad (2.1)$$

where, λ is the wavelength of x-ray, d is the inter planer spacing, θ is the angle of incidence, and n represents the order of diffraction [101]. A schematic diagram illustrating Bragg's law is shown in figure 2.2. In a typical diffraction pattern, intense Bragg peaks can be observed at a certain scattering angle where the constructive interference satisfies Bragg's law. Generally, the number of Bragg peaks in a diffraction pattern depends on the crystal

symmetry of the material. A low crystal symmetry such as monoclinic exhibits a large number of Bragg peaks due to numerous lattice planes, whereas high crystal symmetry such as cubic and tetragonal exhibits fewer Bragg peaks due to the limited number of lattice planes in them. Besides the crystal symmetry, the size and shape of particles also affect the nature of Bragg peaks.

There are three basic components of x-ray diffractometer namely an x-ray generator, a sample holder, and a detector. In an x-ray generator, the filament in a cathode

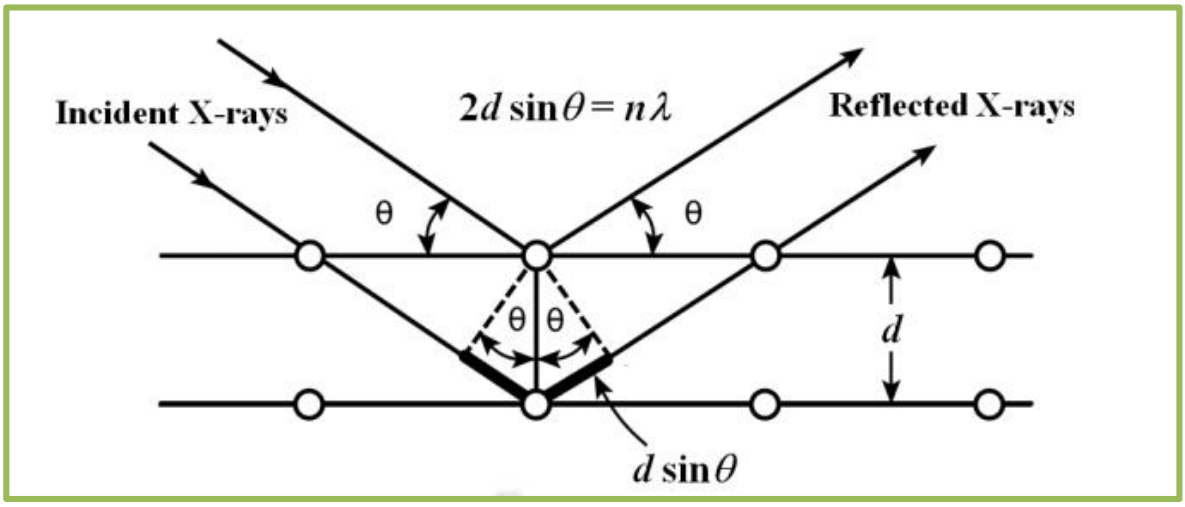

Figure 2.2 A schematic diagram for the Bragg's x-ray diffraction.

tube is heated to produce the electrons which are accelerated by applying the high voltage. The accelerated electrons are then directed towards the target material to bombard it and to produce the characteristic x-ray. Cu is the most commonly used target metal with the characteristic x-rays, K_α of wavelength 1.5481 Å. These characteristic x-rays are collimated and impinge on the sample holder carrying the sample. The diffracted x-rays from the sample are collected by the surrounding x-ray detectors which convert the x-ray signals into the

count rate. Most of the x-ray diffractometer utilizes the Bragg-Brentano para focusing geometry which provides the high intensity of x-ray beam along with the high resolution. It requires a flat surface of sample which helps in the collection of x-ray signals through the detector. In this geometry, the incidence angle between x-ray beam and the sample surface is always half of the detector angle. The sample and detector rotate at the angle θ/min and 2θ/min, respectively. Usually, the x-ray diffraction pattern is acquired in the range of 2θ = 5 – 120^{o}.

In the present thesis work, Rigaku Miniflex makes X-ray diffractometer (Cu K_{α} with λ = 1.54 Å) operating in a Bragg-Brentano geometry was used to acquire the XRD patterns. The x-ray diffractometer was fitted with the graphite monochromator and the x-ray wavelength used was 1.5418 Å. The XRD data was indexed and matched with Joint Committee on Powder Diffraction Standards data (JCPDS) to confirm the phase purity of the samples. The analysis of diffraction patterns was carried out by employing the Rietveld refinement method using the FullProf program[102,103]. Rietveld Refinement probes phase purity of the samples and also gives the crystal structure information such as lattice parameter, atomic position, occupancy, bond length, bond angle, etc [104]. Basically, it uses a non-linear least square method to minimize the difference between the experimental and the calculated XRD patterns. In this method, the background was refined using a polynomial function and a Pseudo-Voigt function was chosen for optimizing the peak shape. Global parameters such as coefficients of background polynomial, scaling factor, FWHM parameters (*u*, *v*, *w*), and the lattice parameters (*a*, *b*, *c*) were mainly varied during the refinement. In addition to the fractional atomic coordinates (*x*, *y*, *z*), isotropic (temperature)

displacement parameters and occupancy values were varied. Here, the occupancy is defined as the multiplicity of the Wyckoff position divided by the maximum multiplicity of the same space group. The occupancy of oxygen was taken as 1 and it was not varied throughout the refinement. The reliability factors like R_p (profile factor), R_{wp} (weighted profile factor), R_{exp} (expected weight factor), and χ^2 (reduced chi-square) were used to evaluate the quality of Rietveld refinement as follows:

$$R_p = 100 \frac{\sum_{i=1,n} |y_i - y_{c,i}|}{\sum_{i=1,n} y_i} \tag{2.2}$$

Here, y_i and y_{ci} denote the experimental and calculated data points, respectively. The total number of data points is given by n.

$$R_{wp} = 100 \left[\frac{\sum_{i=1,n} \omega_i |y_i - y_{c,i}|^2}{\sum_{i=1,n} \omega_i y_i^2} \right]^{1/2} \tag{2.3}$$

Here, $\omega_i = {}^{1}/_{\sigma_i^2}$, with σ_i^2 is the variance of the observation y_i.

$$R_{exp} = 100 \left[\frac{n-p}{\sum_{i=1,n} \omega_i y_i^2} \right]^{1/2} \tag{2.4}$$

Here n and p represent the total number of experimental points and refined parameters, respectively. The total number of degrees of freedom is given by n-p.

$$\chi^2 = \left[\frac{R_{wp}}{R_{exp}} \right]^2 \tag{2.5}$$

The bond lengths/interatomic distances and bond angles were calculated using the optimized fractional coordinates and lattice parameters by using the Vesta program available in the Full Prof suite [102].

2.3.2 Scanning electron microscope (SEM)

The scanning electron microscope is utilized to determine the material's topological and morphological information, primarily showing the surface texture. The sample's surface is bombarded with an electron beam, which ionizes the atoms and causes secondary electrons, loosely bound to the atoms, to be ejected. These secondary electrons typically have low energy levels ranging from approximately 3 to 5 eV and can be easily detected. This information is then utilized to create a three-dimensional image of the sample, and a detector is used to collect these scattered secondary electrons and convert them into an electric signal, which is then passed through a cathode ray oscilloscope (CRO). The high-contrast image formed is displayed on a computer screen, and using suitable detection modes, significant contrast against morphology is obtained. The SEM has a spatial resolution of approximately 10 nm, enabling it to resolve most surface characteristics.

Energy Dispersive X-ray Spectroscopy (EDS)

Energy Dispersive X-ray Spectroscopy, commonly known as EDS or EDX, is an analytical technique used to qualitatively and quantitatively analyze the elemental composition of a compound using X-rays. When an electron beam is incident on the surface of the sample, it ejects electrons, creating a vacancy in a particular energy state. Electrons from a higher energy state fill these vacancies, releasing energy in the form of X-rays that balance the

energy difference between the two states. The energy of these emitted X-rays is characteristic of the element. The detector is composed of a crystal that absorbs the expelled X-rays and measures the relative quantity of released X-rays versus their energy.

In the present work, samples were coated with the extremely thin layer (1.5 to 3.0 nm) of gold layer to make the surface electrically conducting. Then, a field emission gun based scanning electron microscope (FE-SEM) of ΣIGMA, ZEISS was used for recording the images of coated samples. A java-based imaging program, Image J was used for processing and analyzing the FE-SEM images [105].

2.3.3 Transmission electron microscopy(TEM)

The Transmission Electron Microscopy (TEM) technique is an effective way to investigate the morphology, structure, size, and distribution of nanoparticles. The equipment for TEM consists of an electron gun, a vacuum system, electromagnetic lenses, high voltage generator, recording devices, and electronics. TEM has a remarkable resolution of under 0.2 nm, even with a decent amount of tilting of the specimen. Unlike other microscopy techniques, TEM uses electrons of shorter wavelengths to provide high-resolution images. The electron gun assembly and electromagnetic condenser lenses produce a well-focused electron beam, which is accelerated by an anode typically set at 100 KeV compared to the cathode. The beam is restricted by the condenser aperture, which blocks un-collimated electrons. The high-energy (200 KeV and above) collimated beam of electrons hits the specimen and gets scattered depending on its thickness and electron transparency. The objective lens focuses

the scattered electron beam that undergoes a change in phase and amplitude, forming an image on a phosphor screen or charge-coupled device camera.

TEM can operate in two modes: diffraction mode and imaging mode. By changing the excitation of the lenses following the objective lens, modern TEM can switch between these two modes. The TEM image displays well-distributed particles that can be analyzed for their shape and size distribution. Using Image J software, a histogram of particle distribution (particles size vs. number of particles) can be plotted. Fitting the data with Lorantzian distribution provides the average particle size. A selective area electron diffraction (SAED) pattern displays well-concentric rings of different radii. The diffraction rings can be indexed by calculating the inverse of their radii and matching them with the interplanar spacing (d) in reciprocal space of XRD data using Win PLOTR software.

High Resolution Transmission Electron Microscopy (HR-TEM)

This technique, which represents an advancement in TEM imaging, provides atomic-scale information about the crystal structure of a sample. An interference pattern is generated using the scattered and transmitted beams. The resulting HRTEM phase contrast image is typically on the scale of the crystal's unit cell and can achieve high resolution magnifications below 0.1 Å. The electron gun voltage applied is typically 200 kV. The well-defined atomic planes observed with HRTEM can be indexed by calculating their interplanar distances and compared with XRD data to confirm the crystal structure.

To prepare the samples for imaging, 1 milligram of $CeCrO_3$ powder was dispersed in 15 ml of ethanol and sonicated in an ultrasonicator to ensure homogeneous

mixing. A sonicated solution was then drop casted onto a commercial TEM grid (carbon-coated copper grid) and dried in a vacuum oven to evaporate the ethanol before imaging with TEM.

2.3.4 X-ray photo electron spectroscopy (XPS)

XPS, also known as ESCA (Electron Spectroscopy for Chemical Analysis), is a technique used to analyze the chemical state of elements. This method is particularly sensitive to the surface of the material and can provide information about its composition, oxidation state, and valence band structure. A typical schematic diagram of XPS instrumentation is shown in figure 2.3.

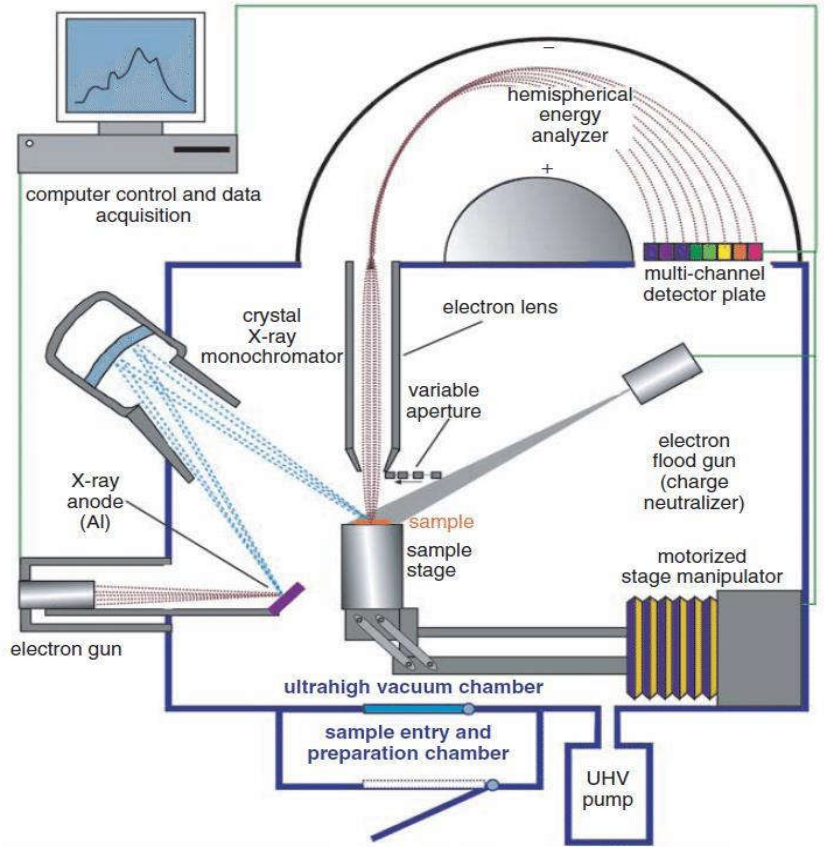

Figure 2.3 The schematic diagram of the XPS instrument.

XPS is based on the photoelectric effect, whereby X-ray photons with energy hν eject electrons from the surface of the sample. The photo excited electrons scatter nearby electrons, losing energy and preventing them from penetrating the specimen. This scattering produces unwanted secondary inelastic background intensity. Only photoelectrons originating from a few tens of angstrom depth can be identified due to the high degree of scattering. The kinetic energy of emitted electrons is given by the equation K.E. = hν – B.E. – Φ, where hν is the energy of the incident X-ray photon, B.E. is the binding energy of the emitted electron, and Φ is the work function. Photoelectrons are produced only if hν ≥ B.E. + Φ. The emitted photoelectrons are identified by their respective kinetic energies and pass through the work function barrier to reach the detector. When the chamber is evacuated to ultra-high vacuum, scattering and collisions between emitted electrons are reduced, increasing their mean free path and allowing them to easily reach the detector. The X-ray photoelectron spectra show the relationship between the frequencies of emitted electrons and their K.E. In this study, the XPS instrument used was from VSW Al-Kα (energy = 1486.6 eV) radiations, and the vacuum level for sample preparation and analysis chambers were ~ 10-8 and ~ 10-9 Torr, respectively. Full energy range scanning was done first, followed by selecting Ce 3d, Cr 2p, O 1s and Fe 2p core level spectra. All observed peaks were calibrated to C 1s peak at ~ 284.6 eV, and XPS data were fitted using software XPS peak 4.2 to determine the exact peak positions, valence states, and area ratio of the elements present in the sample.

2.3.5 Raman Spectroscopy

Raman spectroscopy is a non-destructive technique used for chemical analysis that provides precise information on a material's chemical structure, molecular interactions, and phase formation. It shares similarities with FTIR spectroscopy, as both methods utilize the unique vibrations of a molecule to identify a material. However, Raman spectroscopy can offer additional information on lower frequency modes and vibrations, providing insights into the crystal lattice or molecular structure of the material. This technique relies on light scattering, where a high-intensity laser source interacts with the chemical bonds within the substance. The majority of the scattered light has the same wavelength as the source, known as Rayleigh scattering or elastic scattering. However, some scattered radiation has a loss or gain of energy and varies in wavelength, depending on the material's chemical composition or crystallographic structure. This is known as Raman scattering or inelastic scattering. During Raman scattering, the sample absorbs photons from the laser light and re-emits them with a shifted frequency. This shift indicates information on rotational, vibrational, and other low-frequency transitions within molecules or solids. Figure 2.4 shows the experimental setup used for Raman spectroscopy, which includes a Raman spectrometer, measurement cell, and detector. The laser source is directed towards a dichroic filter, which reflects the beam onto the sample at a 90° angle. The resulting scattered beam of the same wavelength is directed back to the dichroic filter. Only the Raman scattered beam, which has a changed wavelength, can pass through the filter without any alterations. Mirrors are used to guide the measured light to a monochromator, which utilizes a grating to diffract the beam into a narrow range of wavelengths. The photo current from each wavelength is detected and measured. The

Raman spectrometer used in this work includes an argon laser source with a wavelength of approximately 487 nm, and Raman spectra of $CeCrO_3$ samples were recorded between 100 to 800 cm^{-1}.

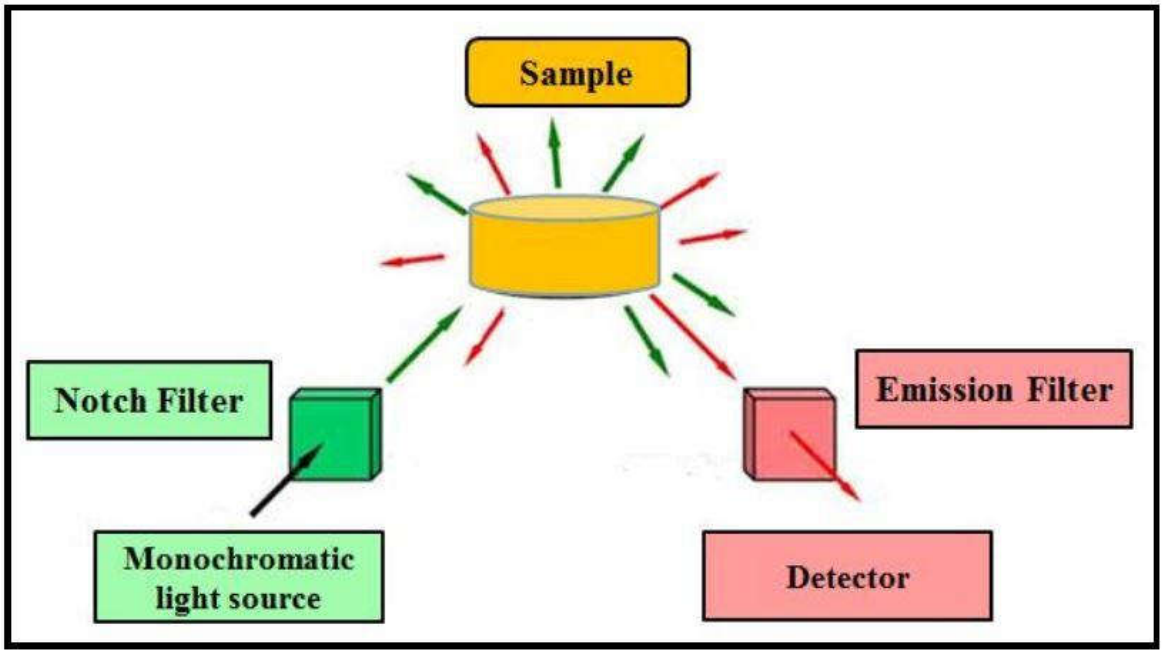

Figure 2.4 Schematic diagram for the simplified setup of Raman spectroscopy.

2.3.6 UV-Visible spectroscopy

The UV-Visible spectrophotometer is a tool that utilizes optical principles to analyze the absorption spectra and band gap of materials. In the case of a powder sample, a double beam spectrophotometer was used, with one beam directed at the sample and the other at a standard reference material, $BaSO_4$ powder. The device was equipped with a photomultiplier tube (PMT) to capture the spectra, with a deuterium lamp serving as the UV light source and a

tungsten lamp serving as the visible light source. The Shimadzu 2600 spectrophotometer shown in Figure 2.5 was used to conduct measurements on powder samples in the diffused

Figure 2.5 UV-Visible Spectrophotometer.

reflectance mode. An integrating sphere assembly was employed to facilitate the measurements. Reflectance values were converted to absorbance values in the 200-700 nm range using the Kubelka-Munk function.

2.3.7 Magnetic measurements

The combination of the Superconducting Quantum Interference Device (SQUID) with the vibrating sample magnetometer (VSM) has proven to be a highly effective method for measuring the magnetic characteristics of diverse materials. By merging the exceptional sensitivity of SQUID with the rapid performance of VSM, the SQUID VSM magnetometer has become a remarkably precise tool for measuring the direct current (DC) moment in relation to variables such as temperature, magnetic field, and time. With the capability to

measure extremely minute moments down to 1×10-15 Tesla, the SQUID magnetometer is a valuable resource for magnetic property analysis. Magnetic Property Measurement System (SQUID, MPMS from Quantum Design, USA) used for measurement is shown in figure 2.6.

Figure 2.6 MPMS-3, Quantum Design (USA) used for magnetic measurement

Which mainly consists of the following parts:

1. Superconducting magnet: The Utilizing a superconducting magnet offers an evident benefit in that it can transmit a considerable electrical current without releasing any heat. This type of magnet is designed in a completely enclosed superconducting circuit, which

enables it to operate in a persistent mode. In this mode, the superconducting circuit is charged with the necessary current and maintains a magnetic field during the measurement without requiring an external power source. To alter the current flow or magnetic field in persistent mode, a persistent-current switch is utilized to briefly interrupt a small portion of the superconducting circuit, allowing the external power source to adjust the current flow. Once the desired magnetic field is achieved, the circuit is closed again and the power supply is disconnected. Superconducting magnets are frequently composed of niobium-based compounds.

2. Sample chamber and holder: A sample holder made of either quartz or copper is utilized to mount the sample, and it is connected to the end of a sample rod. The sample rod is propelled into the sample chamber in distinct increments by a stepper-motor-coil. Typically, the sample chamber is tubular in shape and is pressurized with helium gas to maintain low pressure. The top of the sample chamber serves as an airlock for purging and evacuation procedures.

3. Detection coil: A superconducting detection coil is composed of three coils that are wound from a single piece of superconducting wire, and arranged in a second-order gradiometer format. The coil is located at the core of the superconducting magnet, but positioned outside of the sample chamber. As the sample passes through it, the associated magnetic field inductively couples with the coil. The primary objective of utilizing the gradiometer configuration is to minimize the noise level in the detection coil that may arise due to the strong magnetic field of the magnet.

4. SQUID: The SQUID is an incredibly sensitive device used in magnetometry to measure the magnetic field produced by a sample. It is composed of a closed superconducting loop that contains one or two Josephson junctions in the path of the electrical current. What makes SQUID so remarkable is its ability to detect a magnetic moment as tiny as 10-15 Tesla, while simultaneously being able to function with fields as high as 7 Tesla. It is worth noting that the magnetic field of the sample is not detected directly by the SQUID. Instead, the sample's magnetic moment induces a current in the detection coil as it passes through it. This current passes through a superconducting wire to the SQUID. A variation in the detection coil current induced by vibrating the sample at a fixed frequency under a uniform field produces a corresponding variation in the SQUID output voltage. As the SQUID functions as a highly linear current to voltage converter, any changes in the detection coil current result in proportional changes in the SQUID output voltage. The magnetic moment of the sample is proportionate to the SQUID output voltage. The thin-film form of the SQUID is positioned beneath the sample chamber.

The Magnetic Properties Measurement System (MPMS3) from Quantum Design, USA was utilized in this study to measure the magnetizations of samples as a function of temperature and magnetic field. The measurements were carried out over a range of temperatures between 2 K $\leq$ T $\leq$ 350 K and magnetic fields ranging from -7 Tesla to +7 Tesla. To ensure accurate measurements, any trapped magnetic flux in the superconducting coil was removed by demagnetizing the coil using an oscillatory mode from -70 to +70 kOe at 350 K before the magnetic measurements were conducted.

2.3.8 Time of flight neutron diffraction

Time-of-flight neutron diffraction is a powerful technique for determining the nuclear and magnetic structures of materials. By analyzing the pattern of diffracted neutrons from a sample, researchers can obtain detailed information about the positions and orientations of atoms and magnetic moments within the material. Time-of-flight neutron diffraction is particularly useful for studying magnetic materials, as it allows researchers to measure the magnetic structure with high precision. Neutrons are ideal probes for studying magnetic materials because they have both a magnetic moment and an electric charge, which allows them to interact strongly with magnetic moments within a material. Time-of-flight neutron diffraction is based on the principle that the time it takes for a neutron to travel a certain distance depends on its energy. Neutrons with different energies interact with the sample in different ways, depending on the magnetic properties of the material. In a time-of-flight neutron diffraction experiment for magnetic structure determination, a pulsed neutron source is used to generate a burst of neutrons with a range of energies. The neutrons are directed at a magnetic sample, and the diffracted neutrons are detected by a detector placed some distance away. By analyzing the time-of-flight data, researchers can obtain information about the magnetic structure of the sample. The magnetic structure of a material is described by the positions and orientations of magnetic moments within the material. These magnetic moments can interact with the neutron beam in a variety of ways, depending on the energy and direction of the neutron. By analyzing the pattern of diffracted neutrons, researchers can obtain information about the magnetic moment distribution within the material. This information can be used to determine the magnetic structure of the material, including the

direction and strength of the magnetic moments. Time-of-flight neutron diffraction is particularly useful for studying complex magnetic structures, such as those found in multiferroic materials.